Universiteit
Leiden
The Netherlands

Atmospheres of hot alien Worlds

Brogi, M.

Citation
Brogi, M. (2014, June 5). *Atmospheres of hot alien Worlds*. Retrieved from https://hdl.handle.net/1887/25873

Version:	Publisher's Version
License:	Licence agreement concerning inclusion of doctoral thesis in the Institutional Repository of the University of Leiden
Downloaded from:	https://hdl.handle.net/1887/25873

Note: To cite this publication please use the final published version (if applicable).

Cover Page

Universiteit Leiden

The handle http://hdl.handle.net/1887/25873 holds various files of this Leiden University dissertation.

Author: Brogi, Matteo
Title: Atmospheres of hot alien Worlds
Issue Date: 2014-06-05

1

Introduction

The origin of planetary systems and the existence of life elsewhere in the Universe are arguably among the most fascinating subjects of modern astrophysics. For centuries mankind could only speculate about the existence of planets orbiting stars other than the Sun (exoplanets), and even in relatively modern times the technological challenges for discovering such bodies were too overwhelming. The last two decades revolutionized the field of exoplanets, so that we are currently living the golden era of their discoveries. Thanks to dedicated surveys and telescopes, operating both in space and from the ground, planet hunters have found more than a thousand objects[1], and a sample three times bigger awaits confirmation.

Perhaps the most surprising characteristic of the known exoplanets is their diversity, which has no analogs in the Solar System. Figure 1.1 shows the known planets to date in a semi-major axis, planet mass diagram (a, $M_{\rm P}$). The top-left corner of the diagram pictures a population of giant planets in very close orbits, much closer to their parent star than Mercury is to the Sun, which are called *hot Jupiters*. The existence of this population challenged the main-stream theories of planet formation and evolution at the time of the first discoveries (Mayor & Queloz 1995; Marcy & Butler 1996; Butler et al. 1997), and led to the introduction of planet migration during the early stages of planet formation (Lin et al. 1996; Rasio et al. 1996). A more recent surprise was the discovery of bodies intermediate between the size of the Earth and that of Uranus. Despite no such object is observed around the Sun, they seem to be the most common planets in our Galaxy (Fressin et al. 2013; Petigura et al. 2013).

The two examples above suggest that, in the general picture of planet formation and evolution, our Solar System is uncommon, and must be placed in context by deriving the properties of exoplanets as accurately as possible. These include their masses and radii, the orbital parameters, and the atmospheric structure and composition. Studying exoplanet atmospheres is a crucial task for identifying habitable planets and detecting possible signatures of life, which is one of the ultimate goals of exoplanet sciences.

Up to now, the majority of the exoplanet detections have been achieved by using two indirect methods, namely the radial velocity and transit techniques. The direct detection of a planet, which implies imaging the light of the planet separately from that of the host star, is instead a challenging task, which has only recently been demonstrated to be successful (Chauvin et al. 2005; Kalas et al. 2008; Marois et al. 2008). It is so far limited to young, self-luminous planets in large orbits (tens to hundreds of astronomical units), although state-of-the-art instruments such as SPHERE at the ESO Very Large Telescope (Beuzit et al. 2006) or the Gemini Planet Imager

[1] Source: `exoplanet.eu`

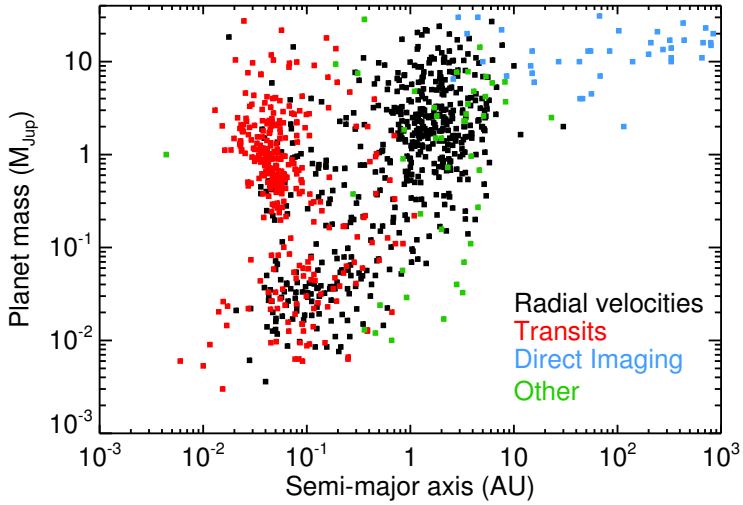

Figure 1.1: The known exoplanets to date in a semimajor axis-mass (a, M_P) diagram. The main discovery techniques are labeled with different colors. We note how transits and radial velocities are complementary in the mass range of giant planets, and how direct imaging is currently limited to massive planets on large orbits.

(Macintosh et al. 2006) will push the detection threshold towards more evolved systems and/or smaller orbits. For the remainder of this introductory Chapter, we will focus on the indirect methods for discovering and characterizing exoplanets.

1.1 Planet properties from transits and radial velocities

Due to the fact that a star and planet both orbit their common center of mass, the presence of the planet can be inferred from the periodic Doppler shift of the stellar spectral lines. By measuring the stellar radial-velocity curve, the orbital semi-major axis, period, and eccentricity can be determined. Due to the unknown orbital inclination i, only a lower limit on the planet mass ($m \sin i$) can be derived, although this thesis presents a novel observational technique to overcome this limit (see Section 1.2.3).

If the orbit of an exoplanet is seen almost edge-on (i.e., the orbit is almost perpendicular to the plane of the sky), the planet crosses the disk of the parent star, which causes a detectable dimming of the stellar light. The depth and the shape of the transit light curve allows us to determine the orbital inclination, the semi-major axis, the orbital period, and the planet radius, but the planet mass remains generally unknown[2].

When a planet is detected both in transit and through radial velocities, the planet

[2]It is sometimes possible to put mass constraints in multiple planets systems, by detecting transit-time variations due to the mutual gravitational interactions between the bodies.

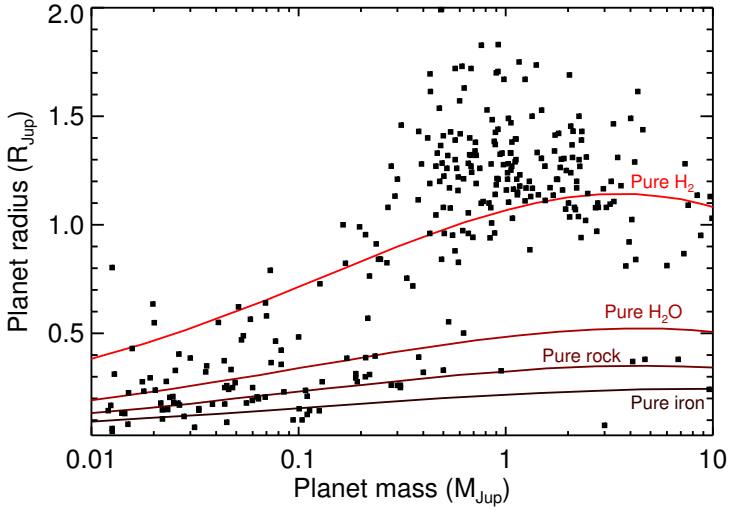

Figure 1.2: The known transiting exoplanets to date in a mass, radius (M_P, R_P) diagram. Theoretical phase curves for compositions ranging from pure iron to pure hydrogen are indicated. We note the significantly higher measured radii of most of the hot Jupiters, with respect to the theoretical values. For small planets and based on the mean density alone, it is impossible to disentangle the atmospheric composition (in particular the mass fraction of H_2) from the planet interior. Finally, the smallest planets below the pure-iron curve have poorly-determined masses and radii, and could therefore move above the pure-iron curve within their 1σ uncertainties.

mass and radius can both be measured. Therefore, the mean planet density can be computed, which is a fundamental parameter to constrain the internal composition of an exoplanet. However, the bulk density alone is often not enough. Figure 1.2 shows the confirmed transiting exoplanets in a mass-radius diagram. Their position in this diagram can be compared with theoretical predictions for the bulk composition, which are shown by the solid-line curves for pure hydrogen, pure water, pure silicate, and pure iron. The first anomaly which is seen is that giant planets have generally inflated radii, the main cause of which is still unclear (see, e.g., Spiegel & Burrows 2013), although it must be related to either extra heating of the planet interior (due to tidal dissipation and/or to ohmic heating) or to its slowed-down cooling (due to extra atmospheric opacity or heating), with stellar irradiation playing an important role in shaping the vertical thermal structure of the atmosphere. In addition, based on their radii and masses alone, it is impossible to robustly infer the internal composition of the smallest exoplanets (Adams et al. 2008). For instance, a water-dominated planet would have the same density as a planet with a rocky core and a hydrogen-rich envelope. The above mass-radius degeneracy also affects the transition between rocky and gaseous planets, although recent work sets it in the range 1.5-2.0 $R_\oplus$ (Marcy et al. 2014; Rogers 2014). These limitations impact our

knowledge of the occurrence of rocky planets, and of their capability to accrete and retain water in close-in orbits. This is tightly connected to exoplanet habitability, and to the search for a true Earth-analog.

In principle, a better understanding of the exoplanet properties can be reached by accessing their atmospheres, which means measuring their composition and vertical structure. For example, it is possible to distinguish between hydrogen-rich and hydrogen-poor planets by measuring their transmission spectrum (Miller-Ricci et al. 2009), a technique presented in more detail in Section 1.2.1. Atmospheres are a key topic of exoplanet science, in particular when searching for habitable planets and the signatures of life (Seager 2013).

1.2 Atmospheric characterization of exoplanets

1.2.1 Atmospheres of transiting planets

The detection of transiting planets (Charbonneau et al. 2000) opened the way to atmospheric characterization, the basic principles of which are shown in Figure 1.3.

Transit: When the planet passes in front of the parent star, part of the stellar disk is masked, causing a decrease $\Delta F_{\rm tr}$ in the total light received from the system ($F_{\rm tot}$). This is proportional to the area of the occulting object:

$$\frac{\Delta F_{\rm tr}}{F_{\rm tot}} = \left(\frac{R_{\rm P}}{R_{\rm S}}\right)^2, \tag{1.1}$$

where $R_{\rm P}$ and $R_{\rm S}$ are the planet and stellar radius respectively, in the approximation that star and planet are spherical. During transit, a small fraction of the starlight also filters through the planet atmosphere, and gets imprinted by its atomic or molecular constituents. Since the opacity of the planet atmosphere changes as a function of wavelength, the size of the opaque planet disk is also changing. Therefore, by measuring the depth of the transit as a function of wavelength, it is possible to construct the *transmission spectrum* of a planet and infer the atmospheric composition.

The modulations in the transmission spectrum have an amplitude $\delta F_{\rm tr}$ proportional to the area of the optically-thin annulus of the planet atmosphere. The thickness of the annulus is typically n = 5-10 times the atmospheric scale height H, which is given by

$$H = \frac{kT}{\mu_{\rm atm} g}, \tag{1.2}$$

where k is Boltzmann's constant, T is the planet temperature, $\mu_{\rm atm}$ is the atmospheric mean molecular weight, and g is the surface gravity of the planet. Therefore, the expected signal is

$$\delta F_{\rm tr} \simeq \frac{(R_{\rm P} + nH)^2 - R_{\rm P}^2}{R_{\rm S}^2}. \tag{1.3}$$

For a typical hot Jupiter, H = 100-200 km, meaning that $\delta F_{\rm tr} \approx 0.1\%$ at wavelengths corresponding to the highest atmospheric opacity.

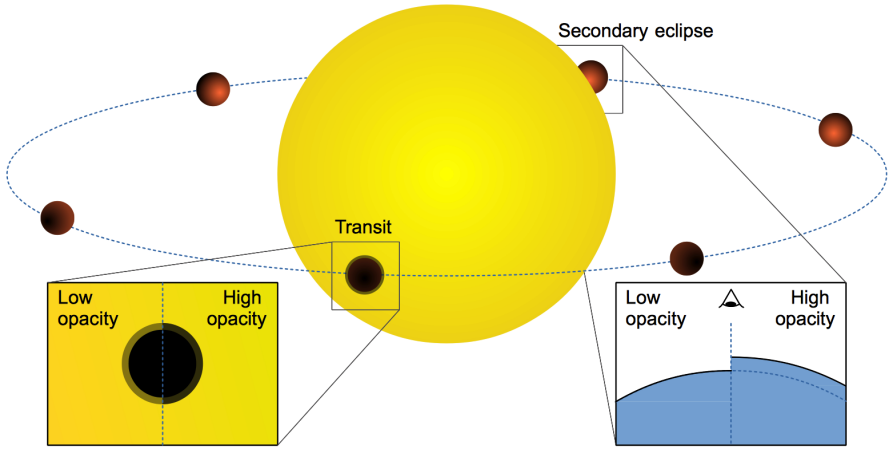

Figure 1.3: Geometry of a transiting planet. A transit occurs when the planet crosses the disk of the parent star, a secondary eclipse when the planet is occulted by the star. The zero planet orbital phase coincides with the mid-transit. The two insets show the effects of changing atmospheric opacity on the measured planet radius in transmission (left inset), and on the atmospheric height probed with secondary-eclipse measurements (right inset). The implications of these variations are further discussed in Section 1.2.1.

Via transmission spectroscopy, atomic sodium (Charbonneau et al. 2002), potassium (Sing et al. 2011a), hydrogen (Vidal-Madjar et al. 2003), carbon and oxygen (Vidal-Madjar et al. 2004) were detected in exoplanet atmospheres. Convincing molecular detections remained elusive until recently, mostly due to the strong debate in the community regarding the analysis of HST/NICMOS and Spitzer/IRAC data (see Section 1.2.2). Thanks to the Hubble/WFC3 (Deming et al. 2013; Mandell et al. 2013) and ground-based, high-resolution spectroscopy (Snellen et al. 2010), we now have a solid evidence of H_2O and CO in transmission spectroscopy. Surprisingly, a considerable fraction of the observed transmission spectra are flat at both optical and near-infrared wavelengths (Gibson et al. 2013; Kreidberg et al. 2014), which likely requires the presence of clouds masking most of the spectral signatures. In addition, featureless optical transmission spectra and slopes consistent with Rayleigh scattering are strongly suggestive of haze (Sing et al. 2011b, 2013).

Secondary eclipses: At superior conjunction, the planet is eclipsed by the star. This also causes a dip in the light curve, because the contribution from the planet reflected light (in the optical) or thermal emission (in the near-infrared) is masked from the observer's view. The depth $\Delta F_{\rm ecl}$ of a secondary eclipse is generally much smaller than the transit depth. In the thermal regime, it can be estimated by

$$\frac{\Delta F_{\rm ecl}(\lambda)}{F_{\rm tot}(\lambda)} \simeq \frac{\mathcal{B}(\lambda, T_{\rm eq})}{\mathcal{B}(\lambda, T_{\rm eff})} \left(\frac{R_{\rm P}}{R_{\rm S}}\right)^2, \tag{1.4}$$

where $\mathcal{B}(\lambda, T)$ is the Planck function at a wavelength λ and for a temperature T. $T_{\rm eq}$

and $T_{\rm eff}$ are the planet equilibrium temperature and the stellar effective temperature, respectively. A guess for the planet equilibrium temperature can be obtained by balancing the incoming stellar flux at the planet position with the outgoing planet emission in the hypothesis of black-body radiation:

$$T_{\rm eq} \simeq T_{\rm eff} \left[\frac{(1-A)R_{\rm S}^2}{4a^2} \right]^{1/4}, \tag{1.5}$$

where A is the Bond albedo (the fraction of reflected starlight at all wavelengths), and a the orbital semi-major axis. For a typical hot Jupiter ($T_{\rm eq} = 1500$ K, $a = 0.05$ AU, $R_{\rm P} = 1.2 R_{\rm Jup}$) orbiting a solar-type star the relative secondary eclipse depth is few times 10^{-3}.

It is important to realize that, by measuring the secondary eclipse depth in the near-infrared, we are essentially probing the temperature of the layer at which the planet atmosphere becomes optically thin. Therefore, by repeating this exercise at various wavelengths, it is possible to detect the presence of atoms or molecules. At frequencies where the planet atmosphere is relatively transparent, we observe the radiation coming from deep layers, ideally from the level where the planet continuum is formed. In the presence of any source of opacity, the atmosphere will become optically thick at higher altitude for an observer looking from the outside (see right inset in Figure 1.3). If temperature decreases with pressure (non-inverted atmosphere), then the planet flux at wavelengths with increased opacity will be lower than the continuum flux (molecular absorption). If temperature increases with pressure (inverted atmosphere), the planet spectrum will show emission features. By measuring the planet flux (i.e., the secondary-eclipse depth) as a function of wavelength it is therefore possible to reconstruct the *dayside spectrum* of a planet. These observations are however very challenging. It is often necessary to measure a temperature difference of less than 500 K, which corresponds to a signal of $\sim 10^{-4}$ in relative photometry. The thermal emission from an exoplanet was detected for the first time from space (Deming et al. 2005; Charbonneau et al. 2005), and only recently the first ground-based detections were reported (de Mooij & Snellen 2009; Anderson et al. 2010). Most of the information about exoplanet dayside spectra comes from observations with the *Spitzer Space Telescope* in the 3.6-24 μm range (see Seager & Deming 2010, for a review). Despite the relatively big sample of about 20 exoplanets, these measurements still do not provide any clear evidence for thermal inversion layers, except in the case of HD 209458 b (Knutson et al. 2008). Moreover, the presence of molecular species (H_2O, CO, and possibly CO_2) has been confidently assessed for two planets only, HD 189733 b and HD 209458 b (Madhusudhan & Seager 2009; Lee et al. 2012; Line et al. 2012).

At optical wavelengths, the planet/star contrast ratio is set by the planet radius, its orbital distance a, and its albedo A:

$$\frac{\Delta F_{\rm ecl}}{F_{\rm tot}} \simeq A \left(\frac{R_{\rm P}}{2a} \right)^2 \tag{1.6}$$

Optical secondary eclipses have been detected thanks to dedicated transit space missions such as *CoRoT* and *Kepler* (Alonso et al. 2009; Snellen et al. 2009; Borucki et al.

2009; Désert et al. 2011; Demory et al. 2011). For the hottest exoplanets, the Wien tail of the thermal emission partially extends to optical wavelengths, complicating the disentanglement of emitted light from reflected light (Coughlin & López-Morales 2012).

Phase curves: Finally, by carefully monitoring the total light from the system as a function of planet orbital phase, it is possible to measure the changing contribution of the night- and the day-side of the planet. This gives insight on the energy balance between the two hemispheres, and it is in general connected to the mechanisms regulating the heat transport in the planet atmosphere (Cowan & Agol 2011). It also allows us to indirectly infer the presence of circulation patterns in the planet atmosphere (Knutson et al. 2012).

1.2.2 Challenges of space- and ground-based observations

Observations of exoplanet atmospheres require detecting signals at the very limit of instrumental possibilities, typically at planet/star contrasts ranging from 10^{-3} to 10^{-5}, normally using instruments not specifically designed for high precision measurements. This means that the level of systematic noise, due to imperfections in the instrument or in the observational strategy, is often comparable to or greater than the planet signal. The removal of such non-Gaussian noise is therefore one of the most crucial aspects of exoplanet atmospheric observations. For this reason, it is not surprising that the first successful studies were conducted from space, where the high instrumental stability and the absence of the contamination by the Earth's atmosphere reduce the impact of systematics.

On the other hand, optical and near-infrared space telescopes have smaller collective areas than their ground-based counterparts. Moreover, space instruments have a lower spectral resolution than ground-based facilities. Before my thesis work, for many of the studied exoplanets, the measured spectra were limited to a few broad photometric bands, encompassing a large number of spectral features. This makes it challenging to identify molecular species, or even to distinguish between emission or absorption features. This level of ambiguity, coupled with the low statistical significance of the detected spectral signatures, limits the determination of the atmospheric composition and vertical thermal structure (e.g., the presence or absence of a thermal inversion layer).

Ground-based telescopes benefit from larger apertures and much higher spectral resolution. On the other hand, absorption or scattering by our own atmosphere, as well as instrumental instability (e.g., variation of detector temperature, pointing, gravity vector, etc.) introduce systematic effects which are hard to remove. This means that in practice the photometric accuracy of ground based observations is usually one order of magnitude lower than for space-based measurements, with the exception of the work presented in this thesis. These limitations particularly affect the observations of secondary eclipses, which would otherwise benefit from the larger collective area of ground telescopes.

For both ground and space-based measurements, there is no general agreement regarding the best strategy for detrending systematic noise in the data. This led to

serious debate in the past years (Swain et al. 2008, 2010; Gibson et al. 2011; Mandell et al. 2011), and resulted in a great effort of the exoplanet community in order to design much more robust observational and data-analysis techniques. The next Section describes a novel technique, which forms the heart of my thesis work, based on ground-based, high-resolution spectroscopy. It is capable to robustly identify molecular species in exoplanet atmospheres, and it is almost unaffected by systematic noise at the typical S/N of current observations.

1.2.3 Ground-based, high resolution spectroscopy

Observations at very high spectral resolution ($R \sim 100,000$) are only possible from the ground, because such high-resolution spectrographs are either too big to be launched in space, or require too large telescope apertures to reach sufficient S/N and be appealing for the broad astronomical community. This means that observations at very high spectral resolution are affected by the contamination of our own atmosphere (telluric contamination), which can be a factor of 10^3-10^4 higher than the signal we are looking for.

On the other hand, high-dispersion observations bring a number of advantages, which are represented in Figure 1.4. It shows a simulated observation of a hot Jupiter around 2.3 μm, targeting a ro-vibrational band of carbon monoxide. The first advantage of high-resolution spectroscopy is that the molecules are resolved into the individual lines, meaning that the identification of molecular features can be achieved robustly by line-matching. In this thesis (Chapters 2, 3, 4, and 6), we make use of cross correlation in order to extract and recognize the signal from a specific molecule. An additional advantage of high-dispersion observations is that the planet orbital motion is detected. In Figure 1.4, the changing Doppler shift of the planet molecular lines, due to the changing orbital radial velocity of the planet, is clearly visible. This allows us to effectively disentangle the telluric contamination (which is not subject to any Doppler-shift) from the planet signal, and to measure the planet radial velocity.

Transiting planets can be observed at high spectral resolution in transmission, or just before and after secondary eclipse, when their dayside hemisphere is facing the observer. More importantly, dayside spectroscopy can be applied to non-transiting planets as well via dayside spectroscopy, the reason being that the planet thermal spectrum is targeted directly. This means that, by coupling the maximum value of the planet and stellar radial velocies (K_P and K_S respectively), it is possible to measure the planet/star mass ratio:

$$\frac{M_P}{M_S} = \frac{K_S}{K_P}, \tag{1.7}$$

which allows us to solve for the true planet mass if the stellar mass is known. Furthermore, the orbital velocity of the planet can be computed from the Third Kepler's Law:

$$v_P = \left[\frac{2\pi G M_S}{P(1 - M_P/M_S)}\right]^{1/3}. \tag{1.8}$$

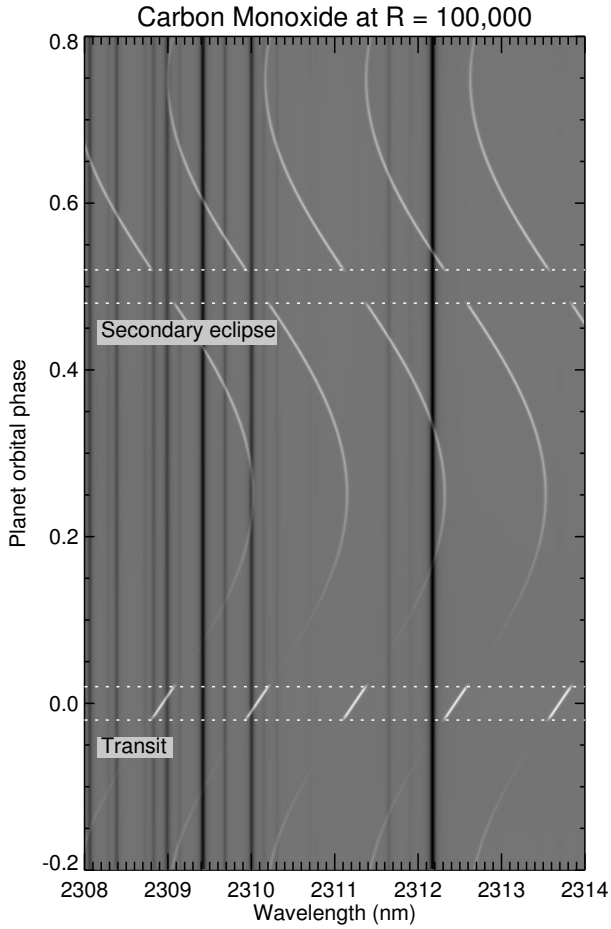

Figure 1.4: Toy model of the spectrum of a close-in, giant exoplanet observed at a spectral resolution of 100,000. Molecular absorption lines from CO in the planet atmosphere (plotted in white) are Doppler-shifted due to the changing component of the planet radial velocity. On the contrary, telluric lines (in black) are stationary in wavelength and can be effectively removed from the data while preserving the planet spectrum, as explained in Section 1.2.4.

This means that the orbital inclination can also be computed as

$$i = \sin^{-1}\left(\frac{K_P}{v_P}\right). \tag{1.9}$$

In this way, atmospheric characterization is also possible for non-transiting planets. This has been pioneered in my thesis work (Chapters 2, 3, and 4).

1.2.4 A novel data analysis

One of the most innovative aspects of our high-dispersion observations is the data analysis, which is summarized here, and described in details in Chapters 2 and 4. The spectral separation between the static telluric absorption and the Doppler-shifted planet signal allows us to self-calibrate the data in the following way. Firstly, we shift all the observed spectra to the same reference frame, which is for these near-infrared observations the telluric frame. With this choice, telluric lines always fall on the same position along the spectral direction (i.e., on the same pixel in the spectra), while the planet signal will appear at a certain wavelength only for a small fractions of the observations, due to the changing radial component of its orbital velocity. Therefore, by fitting the flux in each telluric line as a function of time, and dividing by the fit, we only alter the spectral signatures produced in the Earth's atmosphere, leaving the planet spectrum almost unaffected. The most obvious time dependence in our data is with geometric airmass. Second order effects are given by changes in precipitable water vapor, instrument resolution, etc. Although the normalization above removes any broad-band spectral features and any information on absolute fluxes (including the level of the planet continuum), it also effectively removes telluric absorption, with residual noise typically within $\sim 10\%$ from the photon noise. Furthermore, we preserve the narrow component of the planet spectrum, i.e., the flux ratios between the core of the molecular lines and the planet continuum.

Since the planet signal is typically still buried in the noise at this stage, we utilize cross correlation with model spectra to combine all the molecular lines in the planet's spectrum in one single function (the cross-correlation function, or CCF). We compute the CCF as a function of radial velocity and time. Subsequently, we test all possible radial velocities for the observed planet and we sum the CCF in time, maximizing the total cross-correlation signal. This gives us the best-fitting planet radial velocity, which can be combined with the stellar radial velocity via Equation 1.7, and subsequently utilized to derive the planet mass and orbital inclination.

1.3 Close-in planets and their environment

Close-in giant planets (hot Jupiters) are the ideal test bench for observations of exoplanet atmospheres. Due to their high equilibrium temperatures (T_{eq} = 1500-3000 K) and large radii, they have a favorable contrast with respect to the parent star. This is true not only for the signal from the dayside hemisphere, but also for the signal in transmission, which is increased by the large atmospheric scale height (see Equa-

tion 1.2). Therefore, it is not surprising that the current observations are mostly focused on hot Jupiters, and my thesis work does not break this trend.

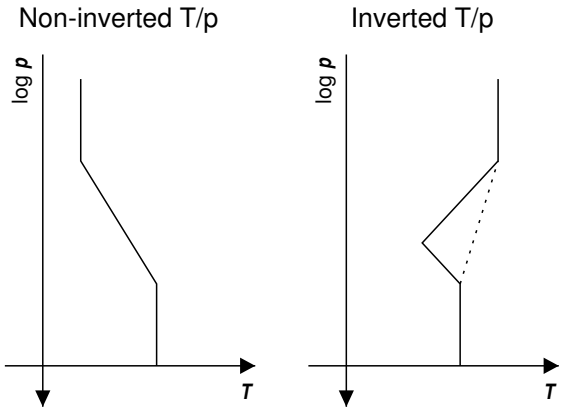

Figure 1.5: Schematic representation of the vertical structure of an exoplanet atmosphere, with (right panel) and without (left panel) a thermal inversion layer. The T/p profiles drawn with a solid line illustrate how temperature changes with pressure. When a thermal inversion layer forms (inverted T/p, right panel), temperature increases with altitude in a certain atmospheric region, while pressure always decreases with altitude. The profiles shown here have the same parametrization as the atmospheric models utilized in Chapters 2, 3, 4, and 6. In most cases, a simpler inverted profile can be assumed with no qualitative difference in the high-resolution model spectra (dashed line, right panel).

The high level of stellar irradiation is thought to be tightly connected to the onset of thermal inversion layers in hot-Jupiter atmospheres. These cause the temperature to increase with altitude in a certain pressure range of the planet atmosphere (see Figure 1.5). The most likely mechanism for thermal inversion is the presence of high-altitude, optical absorbers capable to block the incoming starlight and heat-up the surrounding medium. Fortney et al. (2008) proposed that the level of stellar irradiation could play a role, by preventing these compounds from condensing and rain out from the atmosphere. However, as time passed by, the emerging picture was a general lack of thermal inversion layers, with the best exception to date being HD 209458 b (Knutson et al. 2008). Knutson et al. (2010) suggested that stellar activity could also play a role, with the stellar UV flux capable to photo-dissociate high-altitude absorbers. More recently, Madhusudhan (2012) proposed that carbon-rich planets (i.e., planets having a C/O ratio greater than 1) might naturally lack thermal inversion layers, because the equilibrium abundances of oxides would be extremely small, with all the available oxygen fixed in CO.

The importance of determining the C/O ratio in exoplanet atmospheres is two-fold, as this parameter could also reflect the natal planet environment in the protoplanetary disk (Öberg et al. 2011). The snow-lines of each of the major carbon- and oxygen-bearing molecules are located at different positions in the disk, mean-

ing that the C/O ratio is also expected to vary in both the gas and the condensed phase. This could produce variations in the C/O ratio of the primary atmospheres of forming giant exoplanets. We attempted to measure the atmospheric C/O ratio using ground-based, high-dispersion observations in Chapters 4 and 6. These results complement observations at low spectral resolution, which have so far been unable to put tight constraints on this quantity (Madhusudhan et al. 2011; Crossfield et al. 2012; Line et al. 2014).

1.3.1 From atmospheric escape to catastrophic evaporation

Due to the high level of stellar irradiation, hot Jupiters can also experience atmospheric escape, the detection of which was claimed for neutral atomic hydrogen (Vidal-Madjar et al. 2003; Lecavelier Des Etangs et al. 2010; Linsky et al. 2010) and for neutral or ionized metals (Vidal-Madjar et al. 2004; Astudillo-Defru & Rojo 2013).

Although the timescales of atmospheric loss are still unclear, a planet could in principle lose its entire gas envelope during the main-sequence lifetime of the parent star. A core of a former gaseous planet or a close-in rocky planet could then undergo evaporation, because the equilibrium temperatures of close-in planets are generally higher than the melting point of silicates and possibly of iron. The latest phases of the evaporation occur on a very short timescale, so that it is highly unlikely to observe such a stage (Perez-Becker & Chiang 2013). Nevertheless, a few candidates showing the signatures of evaporation have been found in the *Kepler* database (Rappaport et al. 2012, 2013). One of these peculiar objects is studied in Chapter 5 of this thesis.

1.4 This thesis

This thesis presents observations of the atmospheres of close-in, heavily irradiated planets. These range from ground-based, high-resolution spectroscopy of hot-Jupiter atmospheres to space-based, transit measurements of a putative disintegrating planet.

Chapter 2 presents the first detection of the atmosphere of a non-transiting planet, τ Boötis b, obtained by measuring dayside CO absorption at 2.3 μm via high-resolution spectroscopy with CRIRES at the VLT. By tracing the planet radial velocity, we were able to solve for the planet mass and the orbital inclination, which we found to be $M_{\rm P} = (5.95 \pm 0.28)\ M_{\rm Jup}$ and $i = (44.5 \pm 1.5)$ degrees, respectively. Furthermore, by observing molecular spectral features in absorption, we were able to determine that temperature decreases with altitude in this planet atmosphere. This result appeared in Brogi et al. (2012b).

Chapter 3 presents similar observations applied to 51 Pegasi b, the first exoplanet discovered around a main-sequence star. In this case, H_2O is also detected together with CO, and the measured planet mass is $M_{\rm P} = (0.46 \pm 0.02)\ M_{\rm Jup}$. Interestingly, the orbital inclination is found to be greater than 79.6°, which means that this planet might transit. However, no transit event is observed in any previous photometric monitoring, which sets an upper limit of 82.2° on the inclination. This work was

published in Brogi et al. (2013), and we recently confirmed the water vapor absorption via dayside spectroscopy at 3.2 μm (Birkby et al. in preparation).

Chapter 4 presents again 2.3 μm dayside observations with VLT/CRIRES, which led to the detection of CO and H_2O in the atmosphere of a third non-transiting planet, HD 179949 b. We measured a planet mass of (0.98 ± 0.04) $M_{\rm Jup}$, and an orbital inclination of (67.7 ± 4.3) degrees. Moreover, in this study we show for the first time that it is possible to use high-resolution spectroscopy to measure relative molecular abundances in exoplanet atmospheres and constrain the C/O ratio. In the case of HD 179949 b, our data favors an oxygen-rich atmosphere (C/O < 1) for the planet. These results are currently in press (Brogi et al. 2014).

Chapter 5 shows the quantitative evidence for a disintegrating transiting planet around a star in the *Kepler* field, named KIC 12557548 b. We independently analyzed the *Kepler* photometry and phase-folded the data according to the transit depth. Furthermore, we modeled a trailing tail of dust grains including extinction and scattering, and we showed that such a model exquisitely fits the data. In particular, we were able to quantitatively explain peculiar features of the light curve, such as a flux excess before ingress (due to forward scattering) and a strong asymmetry in the transit shape (due to the tail of dust). By computing realistic scattering functions for silicate grains, we concluded that the typical size of the dust grains is on the order of $\sim 0.1\mu$m. This work appeared in Brogi et al. (2012a).

Chapter 6 pushes high-resolution spectroscopy with CRIRES to the limit, aiming for the detection of the planetary rotation of HD 189733 b, by means of transmission spectroscopy. Not only we detect the combined absorption signal of CO, CO_2, and H_2O, but we also show that the S/N is significantly increases when cross-correlating with template models including a line broadening consistent with a planet rotational velocity of ~ 2.7 km s^{-1}, and corresponding to a rotational period of about 2.2 days, equal to the planet orbital period. This is in line with theoretical predictions that hot Jupiters become tidally synchronized on short timescales after their migration to a close-in orbit.

Finally, in **Chapter 7**, a brief overview of the future perspectives of high-resolution spectroscopy is presented. Among these, we highlight the possibility of detecting oxygen in terrestrial planets around M-dwarfs with future Extremely Large Telescopes, and to study most of the planets around bright stars, which will be found by missions like TESS.

Bibliography

Adams, E. R., Seager, S., & Elkins-Tanton, L. 2008, *ApJ*, 673, 1160

Alonso, R., Guillot, T., Mazeh, T., et al. 2009, *A&A*, 501, L23

Anderson, D. R., Gillon, M., Maxted, P. F. L., et al. 2010, *A&A*, 513, L3

Astudillo-Defru, N. & Rojo, P. 2013, *A&A*, 557, A56

Beuzit, J.-L., Feldt, M., Dohlen, K., et al. 2006, The Messenger, 125, 29

Borucki, W. J., Koch, D., Jenkins, J., et al. 2009, Science, 325, 709

Brogi, M., de Kok, R. J., Birkby, J. L., Schwarz, H., & Snellen, I. A. G. 2014, ArXiv e-prints

Brogi, M., Keller, C. U., de Juan Ovelar, M., et al. 2012a, *A&A*, 545, L5

Brogi, M., Snellen, I. A. G., de Kok, R. J., et al. 2012b, *Nature*, 486, 502

Brogi, M., Snellen, I. A. G., de Kok, R. J., et al. 2013, *ApJ*, 767, 27

Butler, R. P., Marcy, G. W., Williams, E., Hauser, H., & Shirts, P. 1997, *ApJL*, 474, L115

Charbonneau, D., Allen, L. E., Megeath, S. T., et al. 2005, *ApJ*, 626, 523

Charbonneau, D., Brown, T. M., Latham, D. W., & Mayor, M. 2000, *ApJL*, 529, L45

Charbonneau, D., Brown, T. M., Noyes, R. W., & Gilliland, R. L. 2002, *ApJ*, 568, 377

Chauvin, G., Lagrange, A.-M., Dumas, C., et al. 2005, *A&A*, 438, L25

Coughlin, J. L. & López-Morales, M. 2012, *AJ*, 143, 39

Cowan, N. B. & Agol, E. 2011, *ApJ*, 729, 54

Crossfield, I. J. M., Barman, T., Hansen, B. M. S., Tanaka, I., & Kodama, T. 2012, *ApJ*, 760, 140

de Mooij, E. J. W. & Snellen, I. A. G. 2009, *A&A*, 493, L35

Deming, D., Brown, T. M., Charbonneau, D., Harrington, J., & Richardson, L. J. 2005, *ApJ*, 622, 1149

Deming, D., Wilkins, A., McCullough, P., et al. 2013, *ApJ*, 774, 95

Demory, B.-O., Seager, S., Madhusudhan, N., et al. 2011, *ApJL*, 735, L12

Désert, J.-M., Charbonneau, D., Fortney, J. J., et al. 2011, *ApJS*, 197, 11

Fortney, J. J., Lodders, K., Marley, M. S., & Freedman, R. S. 2008, *ApJ*, 678, 1419

Fressin, F., Torres, G., Charbonneau, D., et al. 2013, *ApJ*, 766, 81

Gibson, N. P., Aigrain, S., Barstow, J. K., et al. 2013, *MNRAS*, 428, 3680

Gibson, N. P., Pont, F., & Aigrain, S. 2011, *MNRAS*, 411, 2199

Kalas, P., Graham, J. R., Chiang, E., et al. 2008, Science, 322, 1345

Knutson, H. A., Charbonneau, D., Allen, L. E., Burrows, A., & Megeath, S. T. 2008, *ApJ*, 673, 526

Knutson, H. A., Howard, A. W., & Isaacson, H. 2010, *ApJ*, 720, 1569

Knutson, H. A., Lewis, N., Fortney, J. J., et al. 2012, *ApJ*, 754, 22

Kreidberg, L., Bean, J. L., Désert, J.-M., et al. 2014, *Nature*, 505, 69

Lecavelier Des Etangs, A., Ehrenreich, D., Vidal-Madjar, A., et al. 2010, *A&A*, 514, A72

Lee, J.-M., Fletcher, L. N., & Irwin, P. G. J. 2012, *MNRAS*, 420, 170

Lin, D. N. C., Bodenheimer, P., & Richardson, D. C. 1996, *Nature*, 380, 606

Line, M. R., Knutson, H., Wolf, A. S., & Yung, Y. L. 2014, *ApJ*, 783, 70

Line, M. R., Zhang, X., Vasisht, G., et al. 2012, *ApJ*, 749, 93

Linsky, J. L., Yang, H., France, K., et al. 2010, *ApJ*, 717, 1291

Macintosh, B., Graham, J., Palmer, D., et al. 2006, in Society of Photo-Optical Instrumentation Engineers (SPIE) Conference Series, Vol. 6272

Madhusudhan, N. 2012, *ApJ*, 758, 36

Madhusudhan, N., Harrington, J., Stevenson, K. B., et al. 2011, *Nature*, 469, 64

Madhusudhan, N. & Seager, S. 2009, *ApJ*, 707, 24

Mandell, A. M., Drake Deming, L., Blake, G. A., et al. 2011, *ApJ*, 728, 18

Mandell, A. M., Haynes, K., Sinukoff, E., et al. 2013, *ApJ*, 779, 128

Marcy, G. W. & Butler, R. P. 1996, *ApJL*, 464, L147

Marcy, G. W., Isaacson, H., Howard, A. W., et al. 2014, *ApJS*, 210, 20

Marois, C., Macintosh, B., Barman, T., et al. 2008, Science, 322, 1348

Mayor, M. & Queloz, D. 1995, *Nature*, 378, 355

Miller-Ricci, E., Seager, S., & Sasselov, D. 2009, *ApJ*, 690, 1056

Öberg, K. I., Murray-Clay, R., & Bergin, E. A. 2011, *ApJL*, 743, L16

Perez-Becker, D. & Chiang, E. 2013, *MNRAS*, 433, 2294

Petigura, E. A., Marcy, G. W., & Howard, A. W. 2013, *ApJ*, 770, 69

Rappaport, S., Barclay, T., DeVore, J., et al. 2013, ArXiv e-prints

Rappaport, S., Levine, A., Chiang, E., et al. 2012, *ApJ*, 752, 1

Rasio, F. A., Tout, C. A., Lubow, S. H., & Livio, M. 1996, *ApJ*, 470, 1187

Rogers, L. A. 2014, in IAU Symposium, Vol. 299, IAU Symposium, 247–251

Seager, S. 2013, Science, 340, 577

Seager, S. & Deming, D. 2010, *ARA&A*, 48, 631

Sing, D. K., Désert, J.-M., Fortney, J. J., et al. 2011a, *A&A*, 527, A73

Sing, D. K., Lecavelier des Etangs, A., Fortney, J. J., et al. 2013, *MNRAS*, 436, 2956

Sing, D. K., Pont, F., Aigrain, S., et al. 2011b, *MNRAS*, 416, 1443

Snellen, I. A. G., de Kok, R. J., de Mooij, E. J. W., & Albrecht, S. 2010, *Nature*, 465, 1049

Snellen, I. A. G., de Mooij, E. J. W., & Albrecht, S. 2009, *Nature*, 459, 543

Spiegel, D. S. & Burrows, A. 2013, *ApJ*, 772, 76

Swain, M. R., Deroo, P., Griffith, C. A., et al. 2010, *Nature*, 463, 637

Swain, M. R., Vasisht, G., & Tinetti, G. 2008, *Nature*, 452, 329

Vidal-Madjar, A., Désert, J.-M., Lecavelier des Etangs, A., et al. 2004, *ApJL*, 604, L69

Vidal-Madjar, A., Lecavelier des Etangs, A., Désert, J.-M., et al. 2003, *Nature*, 422, 143